Micromagnetics of derivative ring-shaped nanomagnets

N. Singh,[1,2] S. Goolaup,[2] W. Tan,[2] A. O. Adeyeye,[2,*] and N. Balasubramaniam[1]
[1]*Institute of Microelectronics, 11 Science Park Road, Singapore Science Park II, Singapore 117685, Singapore*
[2]*Information Storage Materials Laboratory, Department of Electrical and Computer Engineering, National University of Singapore, 4 Engineering Drive 3, Singapore 117576, Singapore*
(Received 13 November 2006; revised manuscript received 7 February 2007; published 12 March 2007)

We present a systematic investigation of the magnetization reversal process in derivative ring-shaped nanomagnets. As the transition from onion to vortex state in magnetic rings is through the displacement of the domain wall along the circumference of the ring, we have investigated the effect of removing different segments of the ring structure on the magnetization reversal processes. We observed that the magnetic spin configuration is strongly influenced by the axis that is removed, as confirmed by the magnetic force microscopy studies. Our understanding of the reversal process was aided using micromagnetic simulations, which are in very good agreement with experimental results.

DOI: 10.1103/PhysRevB.75.104407 PACS number(s): 75.75.+a, 75.60.Jk, 75.60.−d

I. INTRODUCTION

There is a growing interest in both the experimental and theoretical studies of magnetization reversal mechanisms in patterned nanomagnets due to their potential application in a wide range of magnetoelectronic devices such as read head sensor, magnetic random access memory, and logic gates.[1–3] The key issue from both the fundamental and technological viewpoints is to understand and control the magnetic properties of individual and interacting elements at reduced dimensions. Recently, the magnetization reversal mechanisms in elliptical,[4,5] square,[6,7] and circular[8,9] nanomagnets of varying sizes and spacing have been widely investigated. Moreover, ring-shaped nanomagnets have attracted a lot of attention[10] due to the presence of a highly stable vortex state which generates the smallest stray field with reduced dipole-dipole interaction, thus allowing them to be a suitable element for high-density data storage devices.

In symmetrical ferromagnetic rings, two distinct states, namely, the "vortex" state and the "onion" state, consisting of two opposite head-on domain walls have been experimentally identified. The transition from the onion state to the vortex state is via the displacement of one of the head-to-head domain walls along one of the axes of the ring and annihilation with the other wall. Notches have been introduced in the ring to pin the domain wall at specific places, leading to an asymmetric magnetization reversal for different applied fields, which is highly dependent on the size of the notch.[11] An alternative method of introducing asymmetry in the ring is by distorting the shape into an ellipse. Castãno *et al.*, observed the formation of an additional state, a 360° domain wall together with the onion and vortex states in elliptical ring Co nanomagnets.[12] Saitoh *et al.*, showed that the chirality of the vortex in nanorings can be controlled by offsetting the inner hole from the middle of the ring.[13] We have recently reported the evolution of magnetic spin states and in-plane magnetic anisotropy in arrays of elongated elliptical $Ni_{80}Fe_{20}$ rings.[14]

In this work, we have carried out a systematic study of the effect of removing different sections of the elongated ring on the magnetization reversal process. Different derivatives of elongated ring-shaped nanomagnets of identical dimensions are fabricated over a large area and characterized. As the transition from the onion to vortex state is through the displacement of the domain wall along the periphery of the ring, the magnetization reversal process is strongly influenced by the missing section of the elongated ring structure. We aided our understanding of the reversal process using two-dimensional micromagnetic simulation. A very good agreement between experiment and simulation was obtained.

II. EXPERIMENTAL DETAILS

In our experiments, large area $Ni_{80}Fe_{20}$ nanomagnets were fabricated on commercially available silicon substrate using deep ultraviolet lithography at 248 nm exposing wavelength. The substrate was first coated with 60 nm of antireflective layer followed by a 480 nm deep UV resist. A Nikon lithographic scanner with KrF excimer laser radiation was used for exposing the resist. Thermal evaporation was used to grow $Ni_{80}F_{20}$ film layer of thicknesses ranging from 20 to 80 nm. The deposition rate for $Ni_{80}Fe_{20}$ was 0.5 Å/s, while the pressure during growth was maintained at 2.0×10^{-6} torr. The magnetic film was removed from the unexposed areas by ultrasonic assisted lift-off in resist thinner OK73. Completion of the lift-off process was ascertained by the color contrast of the patterned $Ni_{80}Fe_{20}$ area and confirmed by inspection under a scanning electron microscope (SEM). The detailed fabrication process is described in Ref. 15. The SEM micrographs of the various arrays consisting of uniformly distributed ring, U-shaped, C-shaped, and half-ring nanomagnets are shown in Fig. 1. The respective inset displays a magnified image of the nanostructures. The nanomagnets are well defined and are uniform over a large area as can be seen in Fig. 1. The long axis length of the ring is 840 nm, while the short axis length is 560 nm. The width of the ring along the long axis is 160 nm and the width along the short axis is 180 nm. The edge-to-edge spacing for the ring was set to 260 nm. In the U-shaped sample, one of the short axes of the ring sample is removed, whereas for the C-shaped sample, one of the long axes is removed. Vibrating sample magnetometer was used to measure the magnetic properties of the nanostructures at room temperature.

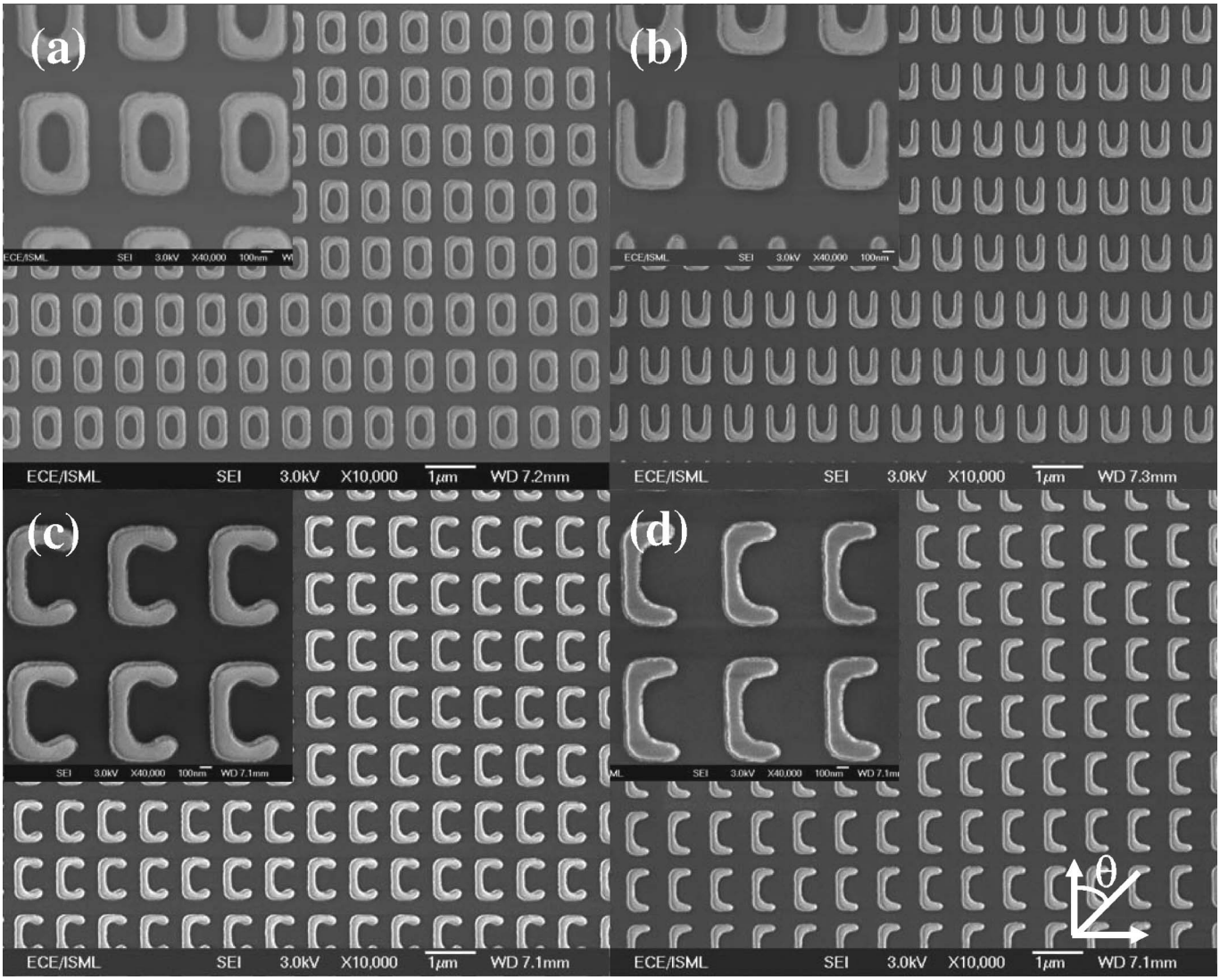

FIG. 1. Scanning electron micrograph of 20 nm thick $Ni_{80}Fe_{20}$ (a) ring, (b) U-shaped, (c) C-shaped, and (d) half-ring nanomagnets. The long axis length is 840 nm and short axis length is 560 nm. The width along the long axis is 160 nm and the width along the short axis is 180 nm. The edge-to-edge spacing is 260 nm.

III. RESULTS AND DISCUSSION

A. Hysteresis measurements

In Fig. 2, we present the representative magnetization loops for 20 nm thick $Ni_{80}Fe_{20}$ nanostructures of different shapes as a function of the field orientation relative to the long axis. We observed that the detailed hysteresis loops are markedly sensitive to both the shape of the structures and the field orientation.

When the field is applied along the long axis of the nanomagnets, a gradual change from two-step to single-step reversal is seen as the structure evolves from full-ring to a half-ring shape, in Figs. 2(a)–2(d). As we have previously reported, this curve is typical of the magnetization reversal process involving the transition from the onion to reverse onion state via the formation of the intermediate vortex state.[14] This has also been reported by other researchers.[11,12]

Interestingly for the U-shaped nanomagnets, we observed a similar *M-H* behavior as for the ring nanomagnets, with the steps in magnetization loops occurring at the same external field as the ring nanomagnets as seen in Fig. 2(b). This implies that the magnetization reversal process is mediated by the same mechanism for both the ring and U-shaped nanomagnets. Due to the absence of one of the shorter axes, only one head-on domain wall forms in the U-shaped nanomagnets. As the field is swept toward positive saturation, the domain wall moves along one of the long axis and is expelled at the tip of the U-shaped structure. This leads to the switching of one of the long axis, along the direction of the applied field, as evidenced by the first step in the *M-H* loop shown in Fig. 2(b). The magnetization in the U-shaped nanomagnets aligns circumferentially along the edge of the structure, similar to the vortex state. The second step in the *M-H* loop corresponds to the reversal of the second long axis comprising the U-shaped nanomagnets. This is ascertained by the equal drop in magnetic moment, following the switching of each long axis, respectively, as seen in Fig. 2(b).

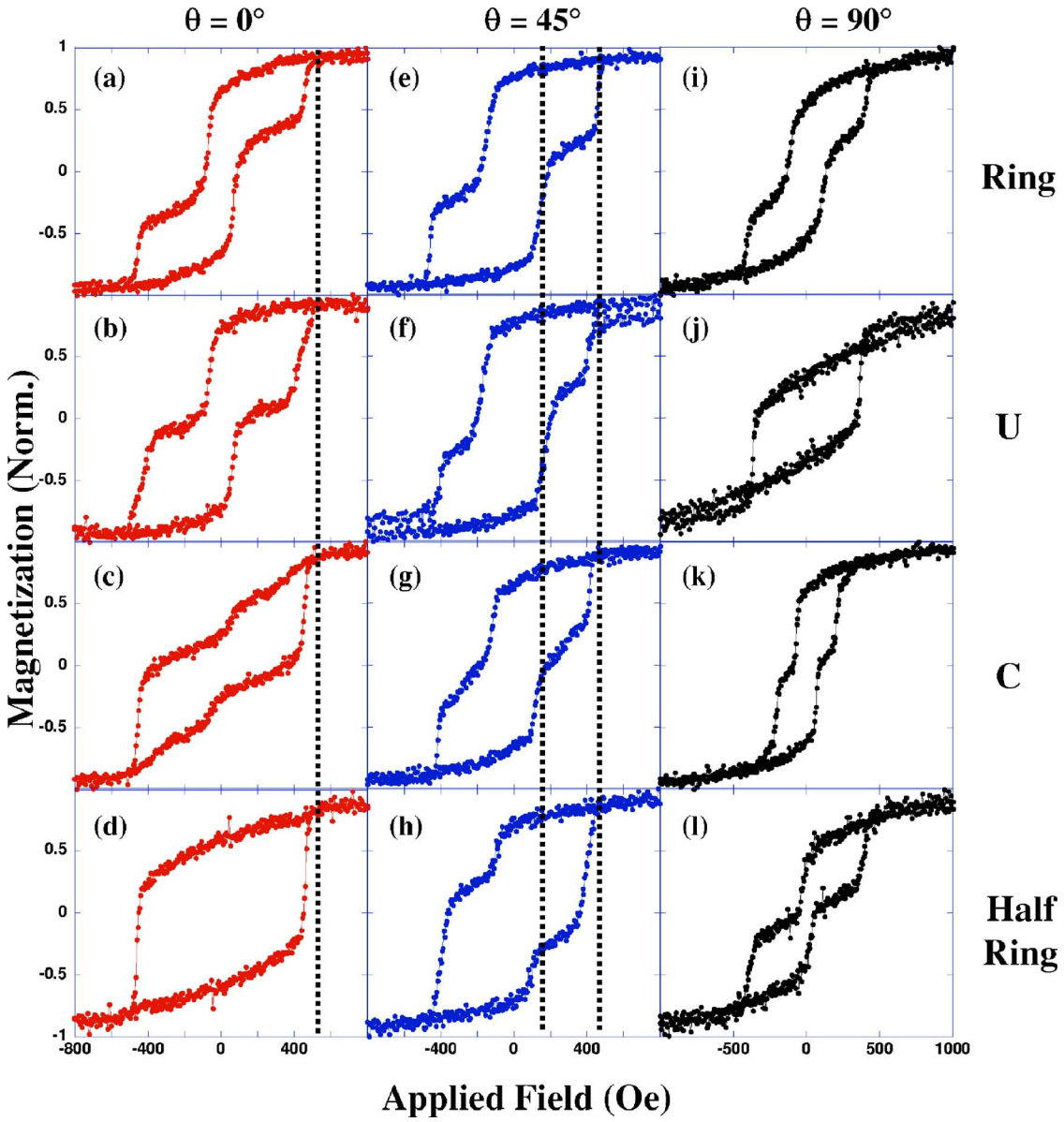

FIG. 2. (Color online) Magnetization loops for 20 nm thick $Ni_{80}Fe_{20}$ nanomagnets for fields applied along the long axis for (a) ring, (b) U-shaped, (c) C-shaped, and (d) half-ring nanomagnets. The corresponding *M-H* loops for field applied at 45° are shown in (e)–(h). The corresponding loops for fields applied along the short axis are shown in (i)–(l).

For the C-shaped nanomagnets, however, we observed a highly sheared two-step *M-H* loop with a coercivity of 350 Oe and a remanent ratio of 0.31, as shown in Fig. 2(c). The loop is characterized by a small step occurring at an external field of 65 Oe, followed by the saturation switching at an external field of 460 Oe. In the C-shaped nanomagnets, with one of the long axes removed, the formation of the head-on domain wall along the short axis leads to a monotonic decrease in magnetization as the applied field is decreased from positive saturation. The sharp increase in magnetization may be due to the switching of the long axis of the C-shaped nanomagnets. This also corresponds to the saturation field of the ring and U-shaped nanomagnets as marked by the dashed line in Figs. 2(a) and 2(b).

The half-ring sample, on the other hand, displays a single-step reversal, with a coercivity of 450 Oe and a remanence ratio of 0.6, as shown in Fig. 2(d). The half-ring sample exhibits the same *M-H* behavior as the C-shaped nanomagnet, due to the absence of one of the long axes. Prior to the sharp switching, the magnetization increases monotonically as the external field is increased. At an external field of 460 Oe, we observed a sharp rise in magnetization leading to saturation. In general, we observed an increase in the coercive field of the structures as the shape is reduced from full to half-ring. This is due to the inability of the structure to sustain a complete circumferential vortex state when one of the axes is removed. Also, the saturation field for all the structure coincides as seen in Figs. 2(a)–2(d). This implies that the overall reversal of the nanomagnets is dominated by the switching of one of the long axes of the nanomagnet.

The corresponding *M-H* loops for the field applied at 45° relative to the long axis of the nanomagnets are shown in

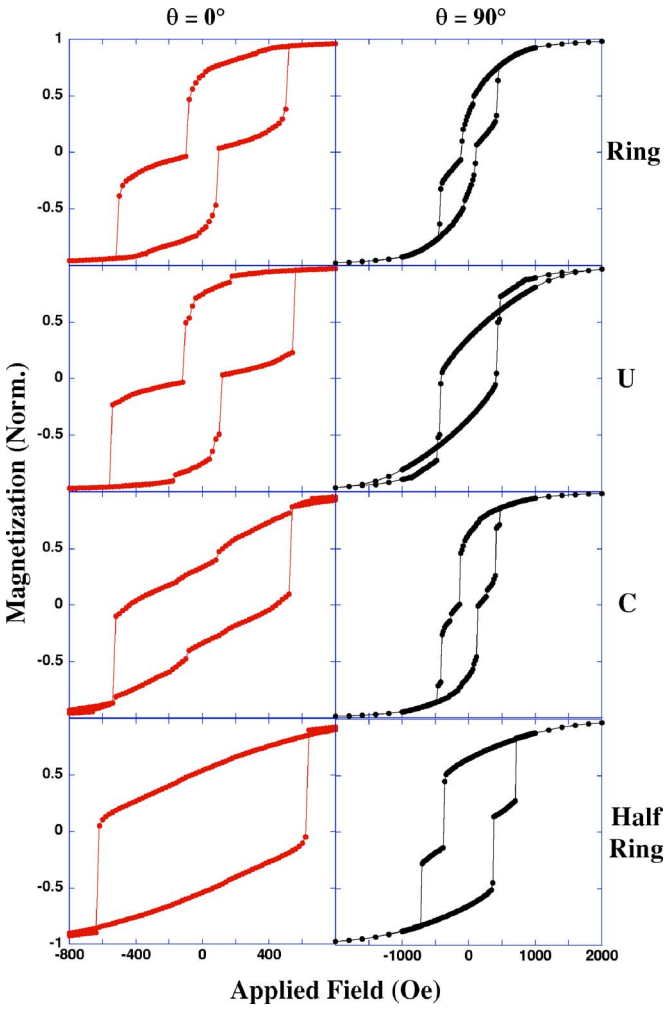

FIG. 3. (Color online) Calculated magnetization loops obtained for single 20 nm thick $Ni_{80}Fe_{20}$ nanomagnet of different shapes, for fields applied along the long axis (θ=0°) and short axis (θ=90°).

Figs. 2(e)–2(h). All the shapes display double-step switching, indicating that similar reversal mechanism process evolves. This is further supported by the fact that magnetization reversal occurs at similar field as marked by the dashed line. For all the nanomagnets, the first switching occurs at an external field of 120 Oe, whereas the second switching takes place at a field of 430 Oe.

Shown in Figs. 2(i)–2(l) are the corresponding *M-H* loops for fields applied along the short axis of the nanomagnets, θ=90°. We observed that all the nanomagnets studied display a double-step reversal, except for the U-shaped sample as shown in Figs. 2(i)–2(l). The *M-H* loop for the U-shaped nanomagnet as seen in Fig. 2(j) is similar to that obtained for the half-ring sample when the field is applied along the long axis, as shown in Fig. 2(d). The marked changes in the magnetization loop as the field orientation is varied imply that shape-induced magnetic anisotropy plays a very dominant role in the magnetization reversal processes.

B. Micromagnetic simulation

To better understand the reversal process in the different nanomagnets, we carried out two-dimensional micromagnetic simulation using the (object oriented micromagnetic framework) OOMMF code from NIST.[16] Due to computational limitation, we have simulated the reversal process of single nanostructures. The parameters used in the simulations are saturation magnetization $M_s = 860 \times 10^3$ A/m, exchange stiffness constant $A = 13 \times 10^{-12}$ J/m, anisotropy constant $K_1 = 0$ J/m^3, and cell size=5 nm. Shown in Fig. 3 are the calculated magnetization loops for single 20 nm $Ni_{80}Fe_{20}$ nanomagnets of different shapes, for fields applied along the long axis (θ=0°) and short axis (θ=90°). The experimental and simulated hysteresis loops show the same field-dependent behavior, and the general features of the calculated *M-H* loops are in very good agreement with the experimental loops presented in Fig. 2. The computed coercivity and saturation fields of the nanomagnets are, however, much larger than the measured values. Micromagnetic simulations tend to overestimate the switching field because thermal fluctuations are not taken into account.

From the micromagnetic spin states for fields applied along θ=0°, we observed that the decrease in the magnetization of the nanoring structure prior to the first drop is due to the formation of the onion state along the short axes. A similar process is seen for the U-shaped sample which lacks one of the short axes of the ring structure. For the C-shaped nanomagnets, we observed that there is no onion state formed in the structure. The reversal is via rotation of the spins at the tip of the C-shaped structure, followed by spin

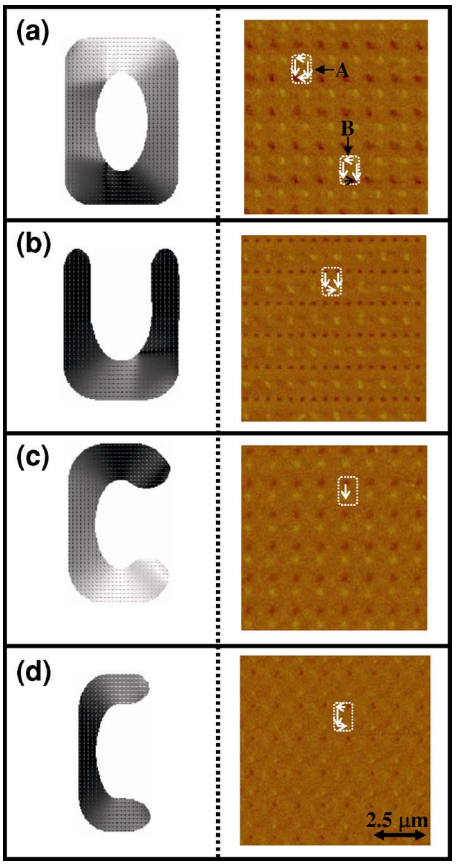

FIG. 4. (Color online) Micromagnetic simulation of the magnetic spin states of the single 20 nm thick $Ni_{80}Fe_{20}$ nanomagnet and the corresponding MFM image over an area of 9×9 μm^2.

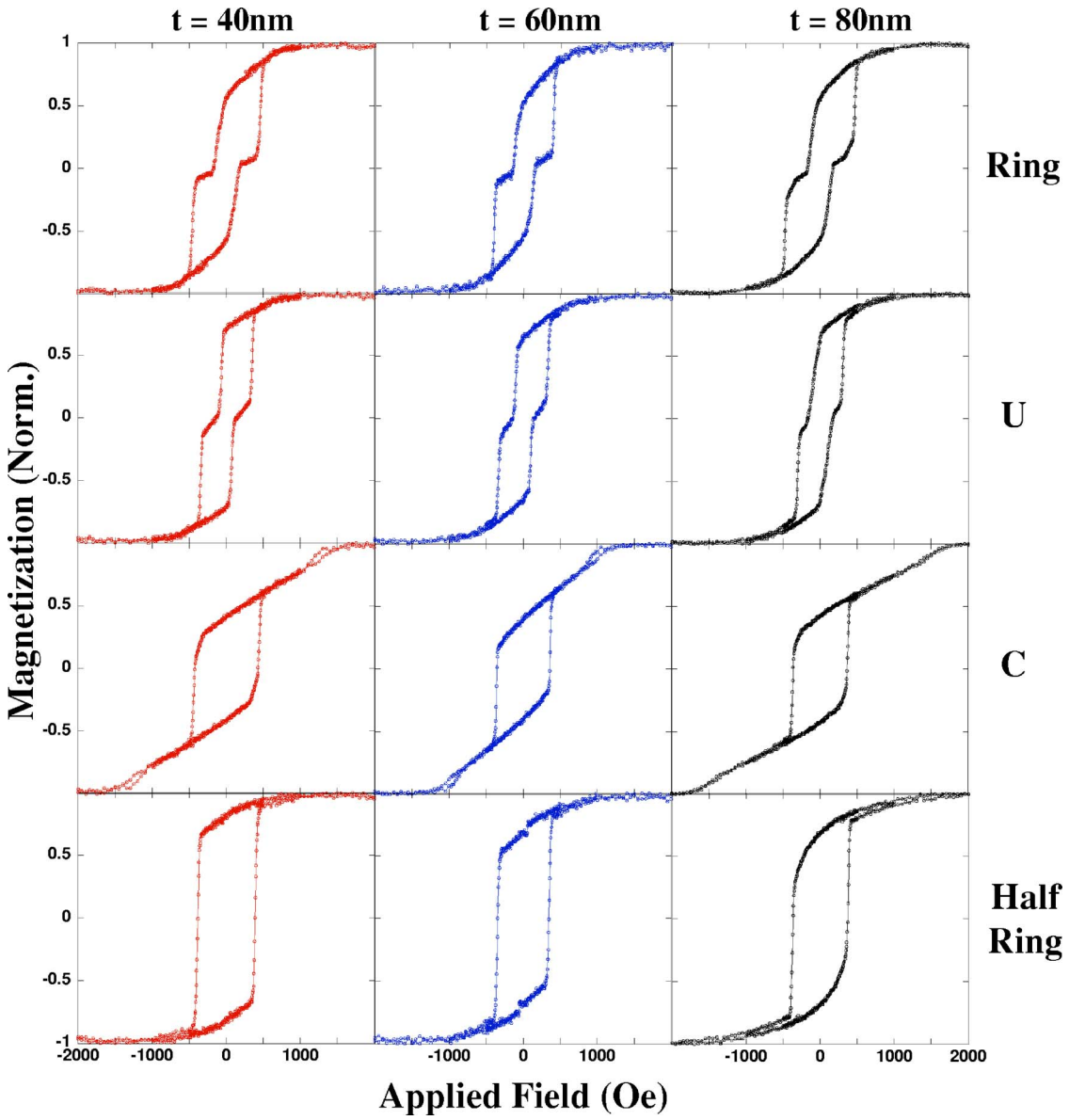

FIG. 5. (Color online) Magnetization loops for fields applied along the long axis (θ=0°) of the nanomagnets as a function of the $Ni_{80}Fe_{20}$ film thickness.

flipping along the field direction for the long axis. A similar process is observed for the half-ring sample.

C. Magnetic force microscopy

To verify our simulation results, we directly imaged the magnetic configuration of the 20 nm $Ni_{80}Fe_{20}$ nanomagnets at remanence, using magnetic force microscopy (MFM). The MFM was performed in the phase detection mode using a CoCr coated tip magnetized along the tip axis. The sample was first magnetized along the long axis (θ=0°) by applying a field of 3 kOe and then reducing the field to 0 Oe. Shown in Fig. 4 are the MFM images of the remanent state of the 20 nm $Ni_{80}Fe_{20}$ nanomagnets and the corresponding magnetic spin state obtained from the micromagnetic simulation.

For the ring nanomagnets, the micromagnetic spin state is characterized by the onion state at the two diagonal corners of the ring as seen in Fig. 4(a). This is in direct agreement with the MFM image, where dark and white spots aligned diagonally from the bottom left to the top right corner of the structure as depicted by configuration A. Interestingly, we observed that one of the ring nanomagnets has adopted the "horseshoe" state. This is due to the switching of one of the short axes, aligning antiparallel to the other axis, as depicted in configuration B. Similar spin state was observed by Vavassori *et al.*[17] in square Permalloy rings for fields applied along the edge direction.

In the U-shaped nanomagnets, the spins along the long axis are aligned along the applied field direction, whereas the spins across the short axis aligned perpendicular to the applied field due to shape anisotropy, as seen in the captured micromagnetic spin sate in Fig. 4(b). This leads to the formation of a head-on domain wall at the bottom right corner of the nanomagnet. The corresponding MFM image displays

a similar spin configuration, with the onion state appearing at the left-bottom corner of the structure. For the C-shaped nanomagnets, the micromagnetic simulation shows that the spins are aligned circumferentially along the structure as seen in Fig. 4(c). As the C shape does not lend itself to a complete flux closure, the resulting MFM image displays a dark and white contrast along the long axis as shown in Fig. 4(c). Similarly for the half-ring structure, the spins are oriented circumferentially around the structure as observed in the spin configuration shown in Fig. 4(d). The MFM image is characterized by white and dark spots at the top and bottom edge of the nanomagnet. As opposed to the C-shaped nanomagnet, the spots on the MFM image occur at the upper and lower edges of the structure, as depicted in the configuration shown in Fig. 4(d). We thus observe that when one of the long axes is removed, the onion state is not formed during the reversal process.

D. Effect of $Ni_{80}Fe_{20}$ film thickness

To understand the effect of the $Ni_{80}Fe_{20}$ film layer thickness on the magnetization reversal of the nanostructures, we carried out a systematic thickness-dependent study. The $Ni_{80}Fe_{20}$ film thickness (t) was varied from 40 to 80 nm, while keeping the lateral dimensions of the structures fixed. Shown in Fig. 5 are the representative M-H loops for the differently shaped nanomagnets as a function of the $Ni_{80}Fe_{20}$ film thickness for fields applied along $\theta=0°$. In general, we observed that the detailed shape of the magnetization loop does not change markedly as the film thickness is increased. While both the ring and U-shaped nanomagnets display double-step reversal as the film thickness is increased, the C-shaped nanomagnets, however, show a very interesting field-dependent behavior. The magnetization loops are characterized by a sudden drop in magnetization, which is sandwiched between two regions of linear monotonic decrease of magnetic moment. Interestingly, the two regions of monotonic decrease in magnetic moment are reversible. We attribute this linear monotonic reduction of magnetization to the spin rotation prior to the switching of the long axis. The half-ring sample, on the other hand, displays a quasirectangular magnetization loop. For all the nanomagnets, we observed that the sharp drop in magnetization prior to saturation coincides for all the thicknesses investigated. As explained previously, this is due to the long axis dominating the reversal process.

IV. CONCLUSION

In summary, we have investigated the magnetic properties of ring-shaped nanomagnets and its derivatives. We found that tailoring of the magnetization reversal process is possible by removing the different segments comprising the ring structure. In elliptical rings, the onion state was not favored when one of the long axes was removed. We aided our understanding of the reversal process using two-dimensional micromagnetic simulation. A good agreement between experiment and simulation was obtained.

ACKNOWLEDGMENT

This work was supported by the National University of Singapore (NUS) under Grant No. R-263-000-283-112.

*Corresponding author. Electronic address: eleaao@nus.edu.sg

[1] M. Hehn, K. Ounadjela, J. P. Bucher, F. Rousseaux, D. Decanini, B. Bartenlian, and C. Chappert, Science **272**, 1782 (1996).
[2] G. A. Prinz, Science **282**, 1660 (1998).
[3] R. P. Cowburn and M. E. Welland, Science **287**, 1466 (2000).
[4] P. Vavassori, O. Donzelli, L. Callegaro, M. Grimsditch, and V. Metlushko, IEEE Trans. Magn. **36**, 2993 (2000).
[5] P. Vavassori, N. Zaluzec, V. Metlushko, V. Novosad, B. Ilic, and M. Grimsditch, Phys. Rev. B **69**, 214404 (2004).
[6] Jing Shi, S. Tehrani, and M. R. Scheinfein, Appl. Phys. Lett. **76**, 2588 (2000).
[7] D. Goll, G. Schütz, and M. Kronmüller, Phys. Rev. B **67**, 094414 (2003).
[8] T. Shinjo, T. Okuno, R. Hassdorf, K. Shigeto, and T. Ono, Science **289**, 930 (2000).
[9] M. Natali, I. L. Prejbeanu, A. Lebib, L. D. Buda, K. Ounadjela, and Y. Chen, Phys. Rev. Lett. **88**, 157203 (2002).
[10] J. G. Zhu, Y. Zheng, and G. A. Prinz, J. Appl. Phys. **87**, 6668 (2000).
[11] J. Rothman, M. Klaui, L. Lopez-Diaz, C. A. F. Vaz, A. Bleloch, J. A. C. Bland, Z. Cui, and R. Speaks, Phys. Rev. Lett. **86**, 1098 (2001).
[12] F. J. Castãno, C. A. Ross, and A. Eilez, J. Phys. D **36**, 2031 (2003).
[13] E. Saitoh, M. Kawabata, H. Harii, H. Miyajima, and T. Yamaoka, J. Appl. Phys. **95**, 1986 (2004).
[14] A. O. Adeyeye, N. Singh, and S. Goolaup, J. Appl. Phys. **98**, 094301 (2005).
[15] N. Singh, S. Goolaup, and A. O. Adeyeye, Nanotechnology **15**, 1539 (2004).
[16] OOMMF is available at http://math.nist.gov
[17] P. Vavassori, M. Grimsditch, N. Novosad, V. Metlushko, and B. Ilic, Phys. Rev. B **67**, 134429 (2003).